Journal of Materials Chemistry A

Accepted Manuscript

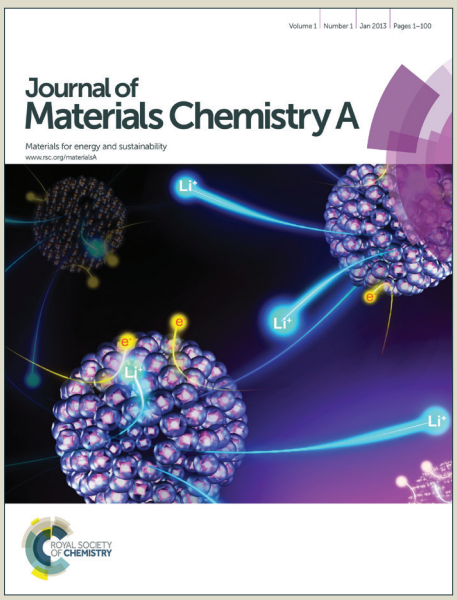

ROYAL SOCIETY OF CHEMISTRY

www.rsc.org/materialsA

Journal Name

ARTICLE

Titanium Doped Niobium Oxide for Stable Pseduocapacitive Lithium Ion Storage and Its Application for 3 V Non-Aqueous Supercapacitor

Received 00th January 20xx,
Accepted 00th January 20xx

DOI: 10.1039/x0xx00000x

www.rsc.org/

Xu Wang,[a] and Pooi See Lee[a]

Developing high energy density supercapacitor is of great importance to the transportation, consumer electronics and micro-grid energy storage sectors. In this contribution, we introduce a titanium doping strategy to enhance the electrochemical performance of orthorhombic phase niobium oxide (T- Nb_2O_5). The Ti doping is able to provide additional redox reaction and reduce the charge transfer resistance during the electrochemical reaction. As a result, Ti doped T-Nb_2O_5 shows pseduocapacitive Li^+ storage capacity of 204.3 mAh g^{-1} and capacity retention of 88.8 % after 1000 cycles at 5C rate. Moreover, a non-aqueous supercapacitor protype based on Ti doped T-Nb_2O_5 and polyaniline-single wall carbon nanotube are fabricated. The 3 V prototype supercapacitor achieves an enhanced energy density of 110.3 Wh kg^{-1} at 150 W kg^{-1}.

Introduction

Supercapacitors are a class of important energy storage devices, which have attracted numerous attention.[1] However, the low energy density of supercapacitor devices has always been bottleneck for their possible applications. Recent development of non-aqueous electrolyte based supercapacitor devices provides an alternative solution for the low energy density issue.[2] In general, the hybrid supercapacitor using organic electrolyte receives the most spotlights among other non-aqueous electrolyte supercapacitor devices. The hybrid supercapacitor consists of a lithium ion battery electrode and a carbon electrode (electrical double layer capacitance, EDLC). The lithium ion battery electrode could be either the positive electrode or negative electrode in the hybrid supercapacitor.[2] Such configuration is able to maximize the device operation potential window. Meanwhile the high capacity of lithium ion battery electrode will elevate the overall device energy density. Thus, the development of a high performance lithium storage electrode is critical for non-aqueous supercapacitor device.

Among all the possible candidates, high rate lithium ion insertion electrode has received considerable attention for the lithium ion storage electrode in hybrid supercapacitor. For example, Chen et al. achieved an energy density of 40 Wh kg^{-1} at 210 W kg^{-1} in a V_2O_5-CNT//activated carbon device.[3] Naoi et al. reported $Li_4Ti_5O_{12}$ nanocrystal on carbon nanofiber//activated carbon with high energy density of 55 Wh kg^{-1} at 100 W kg^{-1}.[4] Aravindan et al. proposed a B-TiO_2 naowires//activated carbon combination to achieve 23 Wh kg^{-1} at 150 W kg^{-1}.[5] Though the results are promising, the recently discovered orthorhombic phase Nb_2O_5 (T-Nb_2O_5) shows much superior Li^+ insertion knetics than the previously investigated materials. T-Nb_2O_5 is found to exhibit intrinsic fast pseudocapacitive Li^+ storage based on an unique intercalation pseudocapacitance.[6, 7] The theoretical capacity of T-Nb_2O_5 is 200 mAh g^{-1}. Comparing with the previous mentioned non-aqueous supercapacitors, carbon coated T-Nb_2O_5 material//activated carbon device shows better energy density at high power densities.[8, 9] However, in those reports, the cycling stability of pristine T-Nb_2O_5 is not satisfactory. It is crytical to coat a thin carbon layer in order to obtain good cycling stability of T-Nb_2O_5. Hence, it compromises the capacity of the T-Nb_2O_5 to around 170 mAh g^{-1}, which deteriorate the development of high energy supercapacitor. Thus, it is of great importance to develop a high capacity T-Nb_2O_5 without sacrificing the capacity meanwhile with stable cycling performance.

On the other hand, in hybrid supercapacitor device, the supercapacitive electrode often relies on the high surface area carbon that can provide electric double layer capacitance. However, the specific capacitance of carbon in organic electrolyte is less than 200 F g^{-1}.[10] The small capacitance of carbon material trades off the high capacity of the Li-ion storage electrode and leads to the low energy density of the two electrode full cell. Meanwhile, the cell voltages of hybrid

[a] School of Materials Science and Engineering, Nanyang Technological University, 639798, Singapore. E-mail:pslee@ntu.edu.sg

† Footnotes relating to the title and/or authors should appear here.
Electronic Supplementary Information (ESI) available: [EDX spectrum of Ti doped T-Nb_2O_5, XRD patterns of T-Nb_2O_5 with different Ti doped ratio, electrochemical performance of activated carbon in 1M $LiClO_4$ in PC, Cycling performance of PANI-SWCNT in 1M $LiClO_4$ in PC]. See DOI: 10.1039/x0xx00000x

supercapacitors are more or less similar, which is around 2.7~3.0 V.[2] Thus, it makes it highly important to elevate the cell capacitance so as to achieve enhanced energy density of hybrid supercapacitor. However, apart from the prevailing usage of carbon electrode, the possiblity of alternative materials as counter electrode is rarely explored. The key requirement of the alternative electrode material is to have high rate capability, compatible in organic lithium electroyte and have similar working potential window like carbon, meanwhile the charge storage property should be much superior than carbon in order to develope a new high energy density device. Polyaniline (PANI) is a redox active conducting polymer, which has been widely studied in aqueous electrolyte as supercapacitor electrode.[11, 12] However, the electrochemical property of polyaniline in organic electrolyte as a supercapacitor electorde is rarely investigated.

Here, we introduce a Ti doping in the T-Nb_2O_5 strategy to achieve better cycling stability without deteriorating the Li^+ storage capacity as well as high rate capability. Meanwhile, pseduocapacitive Li^+ storage behavior is not affected by Ti doping. The Ti doped T-Nb_2O_5 shows a high capacity of 204.3 mAh g^{-1} at 0.5 C while it maintaines 44 % at 25 C. Moreover, the Ti doped T-Nb_2O_5 exhibits good long term cycling stability. On the other hand, the electrochemical propeties of polyaniline coated single wall carbon nanotube (PANI-SWCNT) are examined in organic electrolyte. The PANI-SWCNT shows significantly higher capacitance (650 F g^{-1} at 0.1 A g^{-1}) against activated carbon, meanwhile it preserves resonable rate capability. As a result, the non-aqueous supercapacitor based on Ti doped T-Nb_2O_5// PANI-SWCNT leads to enhanced enegy density of 110.3 Wh kg^{-1} at 150 W kg^{-1}. The idea of replacing activated carbon with high capacitance redox active conducting polymer will be beneficial for development of the next generation non-aqueous supercapacitor device.

Material and methods

Synthesis of Ti doped T-Nb2O5 and T-Nb2O5 materials

A certain amount of $NbCl_5$ was dispersed in the mixed solvent of 15 ml DI water and 5 ml ethylene glycol followed by addition of 40 mM of oxalic acid to give a clear solution. The titanium (IV) butoxide was added in until it is fully dissolved. The ratio between Ti and Nb could was 1:5. Hexamethylenetetramine (HMTA) was dissolved into the above solution to get a 0.1 M concentration. The reaction was carried out at 180 ^oC in autoclave. After a further 14 hours of reaction, the yellow product was collected by centrifugation. The product was washed several times with ethanol and distilled water followed by drying at 60 ^oC for 6 hours. The dried sample was further heat treated at 600 ^oC in air for 3 hrs to give the final product Ti doped T-Nb_2O_5. The T-Nb_2O_5 was synthesized without the addition of titanium (IV) butoxide. The samples were labeled as Ti doped T-Nb_2O_5 and T-Nb_2O_5 respectively.

Synthesis of PANI-SWCNT composite material

SWCNT was first dispersed in the 1 w.t % sodium docylsulfate in 0.5 M H_2SO_4 solution with sonication to give a 0.1 mg ml^{-1} concentration. The SWCNT suspension was then immersed into ice bath and aniline monomer was added into the suspension to give a 13.7 mM concentration. A pre-cooled 4 ^oC ammonium persulfate solution was added dropwise into the above suspension with magnetic stirring and the reaction is further stirred for 12 hrs. The sample was separated by centrifuge and washed with ethanol and DI water several times. The sample was then dried by freeze drying.

Structure Characterizations

The products were characterized using X-ray powder diffractometry (XRD; Shimadzu XRD-6000, Cu Ka radiation) at a scan rate of 2^o min^{-1}, scanning electron microscopy (FESEM; JEOL, JSM-7600F) and transmission electron microscopy (TEM; JEOL, JEM-2010).

Electrochemical characterization

Activated carbon was purchased from XinSen Carbon Industry Co., Ltd, with a BET surface area of 2084.15 m^2 g^{-1}. The working electrode was prepared by mixing 80 w.t% active material, 10 wt.% carbon black, and 10 wt.% polyvinylidene fluoride (PVDF) in NMP. The electrochemical properties of sample T-Nb_2O_5 and sample Ti doped T-Nb_2O_5 were tested in CR2032 Coin cell assembled in an Ar filled glovebox with Li disk as both reference and counter electrode, and 1 M $LiPF_6$ dissolved in 1:1 v/v mixture of ethylene carbonate/diethyl carbonate (EC/DEC) was employed as the electrolyte. The electrochemical properties of PANI-SWCNT composite material were tested in three electrode cell in ambient environment with Ag/AgCl as the reference electrode and a piece of Pt as the counter electrode. 1 M $LiClO_4$ dissolved in propylene carbonate was employed as the electrolyte.

Supercapacitor devices were assembled in an Ar filled glovebox using Ti doped T-Nb_2O_5 as anode and activated carbon or PANI-SWCNT composite material as cathode. The device was assembled based on the optimum mass ratio in CR2032 coin cell in Ar filled glovebox using 1 M $LiClO_4$ dissolved in propylene carbonate as electrolyte. A piece of cellgard battery separator was applied as the separator. The cyclic voltammetry and galvanostatic charge-discharge tests of hybrid device were conducted using Autolab PGSTAT 30 potentiostat from 0~3 V.

Results and discussion

Structural characterization

T-Nb_2O_5 sample and Ti doped T-Nb_2O_5 sample were prepared through hydrothermal reaction followed by heat treatment of 600 ^oC in air. The X-ray diffraction was used to characterize the phase and crystal structure of the pristine T-Nb_2O_5 sample and Ti doped T-Nb_2O_5 sample. As shown in Figure 1a, the diffraction peaks of T-Nb_2O_5 sample match well with PDF # 030-0873, while the main diffraction peaks from Ti doped T-Nb_2O_5 also agrees with the T-Nb_2O_5 sample. Meanwhile, there

are shift of diffraction (001) (180) (181) peak positions in the Ti doped T-Nb_2O_5 sample to higher degrees (~0.26°, 0.14° and 0.26°, respectively). Furthermore, as shown in Figure S1, the modelling of Ti doped T-Nb_2O_5 sample indicates the lattice parameters to be a=6.13 Å, b=28.815 Å, c=3.87 Å. There values are smaller than the a=6.175 Å, b=29.175 Å, c=3.93 Å of pristine T-Nb_2O_5. It suggests the successful doping of foreign cation and the reduction in lattice parameters owing the smaller cation diameter of Ti^{4+}.

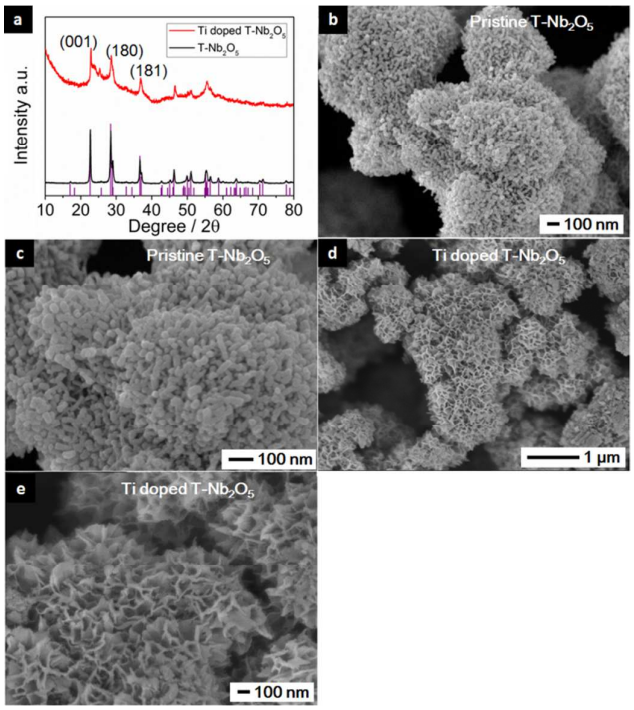

Figure 1. (a) XRD of sample T-Nb_2O_5 and sample Ti doped T-Nb_2O_5; (b) and (c) SEM images of sample T-Nb_2O_5 at different magnifications; (d) and (e) SEM images of sample Ti doped T-Nb_2O_5 at different magnifications.

The chemical existence of Ti was confirmed by EDX as shown in Figure S2a~S1d. From the EDX result, the Ti content in the Ti doped Nb_2O_5 sample is tested to be around 19.4% of the total metal ion content. Furthermore, the Ti:Nb starting ratio of 1:5 is the maximum Ti doping ratio attainable. Higher Ti ratio will lead to phase change under the same synthesis condition, as shown in Figure S2e. Thus, we choose the Ti:Nb=1:5 ratio for the sample preparation in the following characterizations. Figure 1b shows the SEM images of T-Nb_2O_5 sample, where the sample consists of a few micrometers sized particles. These particles are assembled by nanorods with non-conformal size distribution, as shown in Figure 1c. However, the nanorods are seriously agglomerated. Additionally, distinct difference in morphology can be observed when Ti element is incorporated into T-Nb_2O_5. The morphologies of Ti doped T-Nb_2O_5 sample changes from nanorod assemblies into nanoflake assemblies, as shown in Figure 1d. At a closer observation in Figure 1e, the nanoflakes show abundant voids between adjacent structures with no agglomerations. Meanwhile, the nanoflake shows small thickness, which is less than a few tens of nanometers.

More detailed structural study was carried out using Transmission Electron Microscope (TEM). As shown in Figure 2a, it can be clearly seen that T-Nb_2O_5 sample is assembled by short nanorods with irregular lengths and diameters. The length of nanorods is generally less than 100 nm. While the resolution TEM image in Figure 2b shows the clear lattice fringes of the nanorod, showing its single crystalline nature. The crystal lattice spacing in Figure 2b is measured to be 0.212 nm, corresponding to spacing between the (2,10,0) plane in Ti-Nb_2O_5. The TEM images of Ti doped T-Nb_2O_5 sample are shown

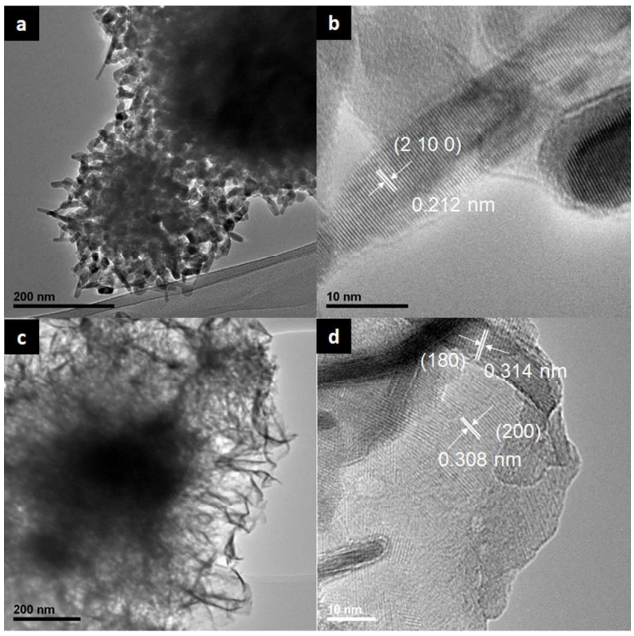

Figure 2. (a) and (b) TEM images of sample T-Nb_2O_5 at low magnification and high magnification; (c) and (d) TEM images of sample Ti doped T-Nb_2O_5 at low magnification and high magnification.

in Figure 2c and d. In Figure 2c, it can be observed that Ti doped T-Nb_2O_5 sample shows distinct difference in the microstructure comparing with the pristine T-Nb_2O_5 sample. The Ti doped T-Nb_2O_5 sample is assembled by dozens of nanoflakes over 200 nm in lateral dimension. Detailed observation of nanoflake under high resolution TEM is shown in Figure 2d. It can be observed that there are multiple crystal domains coexisting in the one nanoflake. Some representative areas show lattice fringes with different orientations, suggesting the polycrystalline nature of the Ti doped T-Nb_2O_5 sample. The lattice spacings are measured to be 0.314 nm and 0.308 nm, corresponding to the lattice spacing of (180) plane and (200) plane respectively.

Electrochemical characterization

Cyclic voltammetry was first used to investigate the electrochemical behavior of different samples. Typical CV curves at 0.1 mV s^{-1} of sample T-Nb_2O_5 and sample Ti doped T-Nb_2O_5 are shown in Figure 3a and b. In Figure 3a, the anodic peaks at 1.50 V and 1.81 V can be attributed to the reduction of Nb^{5+} to Nb^{4+} and Nb^{4+} to Nb^{3+} (Li^+ intercalation)

subsequently, while the broad cathodic peaks centered at 1.75 V are the result of Li^+ deintercalation from Nb_2O_5, as shown in equation 1.[7, 13]

$$xLi^+ + xe^- + Nb_2O_5 \leftrightarrow Li_xNb_2O_5 \quad (1)$$

In Figure 3b, the CV curve of sample Ti doped T-Nb_2O_5 shows a different scenario. There is only one broad anodic peak at 1.57 V, while the cathodic peak is centered at 1.77 V. In addition, a small hump at 2.0 V is also observed. The small hump at 2.0 V and merge of anodic peak can be attributed to the additional redox reaction between Ti^{4+} and Ti^{3+}.[14]

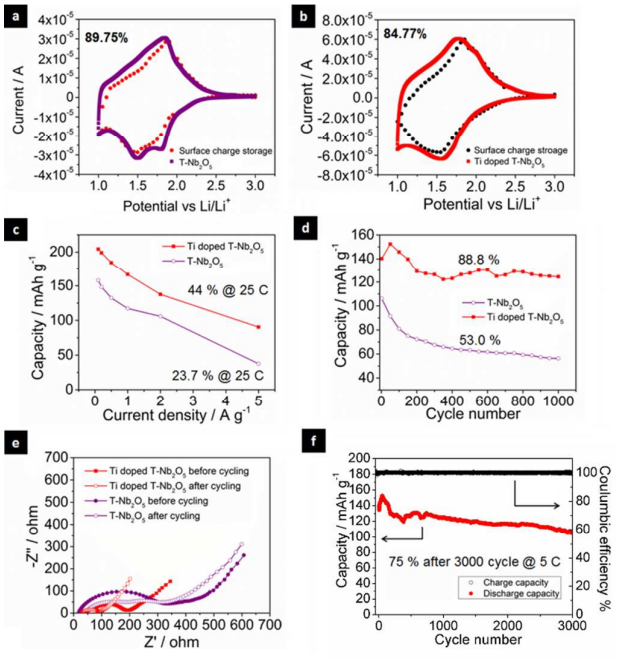

Figure 3. (a) CV curve of sample T-Nb_2O_5 at 0.1 mV s^{-1} and the red dots show the surface charge storage; (b) CV curve of sample Ti doped T-Nb_2O_5 at 0.1 mV s^{-1} and black red dots show the surface charge storage; (c) Relationship between capacity and current density of sample T-Nb_2O_5 and Ti doped T-Nb_2O_5; (d) capacity retention of sample T-Nb_2O_5 and Ti doped T-Nb_2O_5 during 1000 cycles at a current density of 1 A g^{-1}(5 C); (e) Nyquist plots of sample T-Nb_2O_5 and Ti doped T-Nb_2O_5 before and after cycling tests; (f) capacity retention of Ti doped T-Nb_2O_5 during 3000 cycles at a current density of 1 A g^{-1}(5 C).

The behaviors of charge storage of the two samples were further examined using scan rate dependent analysis at 0.1, 0.2, 0.3, 0.4 and 0.5 mV s^{-1}. The current obtained during cyclic voltammetry consists of two parts: non-diffusion controlled redox reaction current (surface charge storage and pseudocapacitive charge storage) and diffusion controlled redox reaction current.[15] In fact, the surface redox reaction current has the linear relationship with the experiment scan rate, that is i=a v. On the other hand, the diffusion controlled redox reaction current has the linear relationship with the square root of the experiment scan rate, that is i=b $v^{1/2}$. Overall, the experiment current recorded during tests can be expressed in equation 2 as:

$$i = a\,v + b\,v^{1/2} \quad (2)$$

which can be transformed into equation 3:

$$i/v^{1/2} = a\,v^{1/2} + b \quad (3)$$

By using scan rate dependent analysis, it is able to determine the coefficients of a and b. In this way, it is able to distinguish between the non-diffusion controlled charge storage and diffusion controlled charge storage at test scan rates. The results of non-diffusion controlled current during CV test at 0.1 mV s^{-1} is shown in the dotted lines in Figure 3a and b respectively. The surface charge storage of sample T-Nb_2O_5 is 89.75 % of the total charge storage, while the surface charge storage of sample Ti doped T-Nb_2O_5 is 84.77 %. As have been demonstrated in previous studies, the orthorhombic phase Nb_2O_5 shows pseudocapacitive Li^+ insertion charge storage behaviour.[6, 7] The Ti doped T-Nb_2O_5 may observe the similar charge storage mechanism, as there is no obvious charge storage behaviour change observed from Figure 3a and 3b. This property is definitely beneficial for high rate capability energy storage. For Ti doped T-Nb_2O_5 here, the surface charge storage ratio is similar with pristine T-Nb_2O_5. Thus, the Ti doped T-Nb_2O_5 sample is also estimated to possess high rate capability.

The relationships between capacity and current density of sample T-Nb_2O_5 and Ti doped T-Nb_2O_5 sample are shown in Figure 3c. The Ti doped T-Nb_2O_5 sample shows much enhanced Li^+ ion storage capacity of 204.3 mAh g^{-1} comparing with the 157.9 mAh g^{-1} of pure T-Nb_2O_5 sample at 0.1 A g^{-1} (0.5 C). In addition, the rate capability of sample Ti doped T-Nb_2O_5 is superior than sample T-Nb_2O_5. When the current density increases to 5 A g^{-1} (25 C), the capacity remains 44 % for sample T-Nb_2O_5 and 23.7 % for sample T-Nb_2O_5. The long term cycling stability of both samples are further examined at 1 A g^{-1} (5 C) for 1000 cycles. The cycling tests were performed on the cells after a few cyclic voltammetry tests. The testing current and cycle times are considered challenging for most Li^+ ion storage electrodes. The capacity of T-Nb_2O_5 sample experiences fast degradation during the first 200 cycles, which shows similar trends with other works.[16] Eventually, the capacity remains only 53.0 % after 1000 cycles. However, the capacity of Ti doped T-Nb_2O_5 sample remains 88.8 % after 1000 cycles, which suggests much improved stability of T-Nb_2O_5 material by Ti doping. In the first hundred cycles for Ti doped T-Nb_2O_5, the increasing of capacity may be due to the activation of the electrode materials. To further investigate the electrochemical property differences of sample T-Nb_2O_5 and sample Ti doped T-Nb_2O_5, electrochemical impedance spectrum (EIS) is performed before and after cycling tests of both samples. As shown in Figure 3e, before cycling test, sample Ti doped T-Nb_2O_5 shows distinct smaller semi-cycle diameter comparing with the sample T-Nb_2O_5. It suggests the much smaller charge transfer resistance from the faradic reaction.[17] The reduction in the charge transfer resistance of Ti doped T-Nb_2O_5 could be due to the lithium insertion into the Ti

doped T-Nb_2O_5 resulting in better electronic conductivity.[18] This reduction in charge transfer resistance is beneficial for better rate capability of sample Ti doped T-Nb_2O_5. Moreover, after long term cycling, the charge transfer resistance of sample Ti doped T-Nb_2O_5 is greatly reduced. On the other hand, the charge transfer resistance of sample T-Nb_2O_5 is more or less the same after long term cycling test. The reduction in the charge transfer resistance in sample Ti doped T-Nb_2O_5 after cycling may be due to the activation process of the material. More prolonged cycling test for sample Ti doped T-Nb_2O_5 is performed for 3000 cycles. As shown in Figure 3f, the capacity of sample Ti doped T-Nb_2O_5 remains 75 % after 3000 cycles, while the coulombic efficiency remains almost 100 % during the cycling. Such cycling stability is greatly enhanced comparing with previous pristine Nb_2O_5 materials.[16, 19]

Structural and electrochemical characterization of PANI-SWCNT composite material

PANI-SWCNT sample was prepared by chemical oxidation method. The SEM images of PANI-SWCNT composite material at different magnifications are shown in Figure 4a and b. The PANI is uniformly coated onto the SWCNT, while there is no obvious observation of PANI forming large agglomerates. It therefore suggests the conformal formation of PANI on the SWCNT surface. Meanwhile, the diameter of the PANI coated SWCNT is around 50 nm, which is of great benefit for shortening the ion diffusion length.

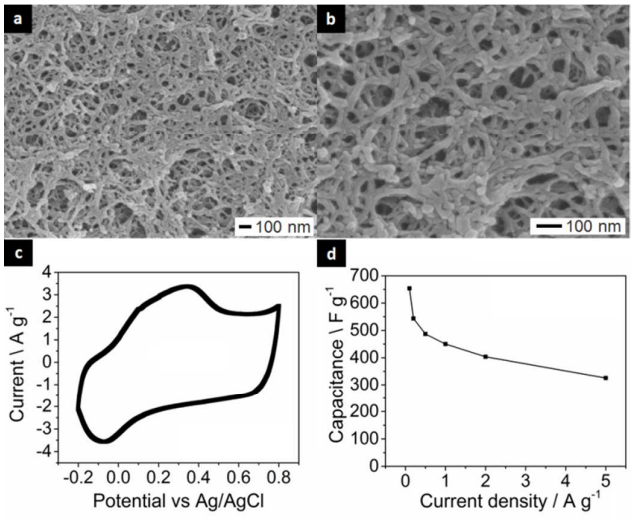

Figure 4. (a) and (b) SEM images of PANI-SWCNT sample at different magnifications; (c) CV curves of sample PANI-SWCNT at 0.2 mV s^{-1}; (d) relationship between capacitance and current density of sample PANI-SWCNT.

The cyclic voltammetry was first carried out to examine the electrochemical behavior of the PANI-SWCNT composite material from -0.2 to 0.8 V vs Ag/AgCl (3~4 V vs Li/Li^+). As shown in Figure 4c, there is a pair of redox peaks between -0.1~0.4 V, which includes the conversion between the fully reduced leucoemeraldine base to the partially oxidized emeraldine and between emeraldine and pernigraniline[20]. Galvanostatic charge-discharge tests were performed to determine the capacitance of PANI-SWCNT composite material. The corresponding charge-discharge curves are shown in Figure 4d. The well symmetric triangular shape charge-discharge curves indicate the well-defined capacitive behavior of PANI-SWCNT composite material. The capacitance of composite material is calculated according to the equation 4:

$C_{sp}=I\Delta t/M\Delta V$ (4)

where I is the discharge current, Δt is the discharge time after IR drop, M is the mass of active material, and ΔV is the test potential window. The specific capacitance of PANI-SWCNT composite material is 650 F g^{-1} at 0.1 A g^{-1}, while it maintains 300 F g^{-1} at 5.0 A g^{-1}, showing good rate capability in organic electrolyte. This value is significantly higher than the capacitance of commercially available activated carbon as shown in Figure S3.

Assemble of supercapacitor device and electrochemical property

The supercapacitor device was assembled using Ti doped T-Nb_2O_5 and PANI-SWCNT (or activated carbon) based on the charge balancing principle in equation 5[21, 22]:

$Q_{Ti\text{-}Nb2O5} = Q_{PANI\text{-}SWCNT}$ (5)

Where $Q_{Ti\text{-}Nb2O5} = m_1 \times 204.3$ mAh $g^{-1} = m_1 \times 735.48$ C g^{-1}, while $Q_{PANI\text{-}SWCNT} = m_2 \times 653.65$ F $g^{-1} \times 1$ V $= m_2 \times 653.65$ C g^{-1}. Thus, $m_1:m_2=1:1.12$. The mass ratio between Ti doped T-Nb_2O_5 and activated carbon can be calculated likewise.

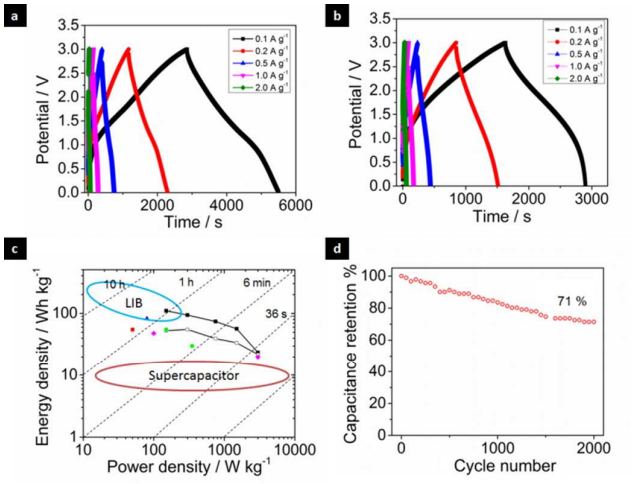

Figure 5. (a) Galvanostatic charge-discharge tests of Ti doped T-Nb_2O_5//PANI-SWCNT supercapacitor device; (b) galvanostatic charge-discharge tests of Ti doped T-Nb_2O_5//activated carbon supercapacitor device; (c) Ragone plot of Ti doped T-Nb_2O_5//PANI-SWCNT supercapacitor device (■), Ti doped T-Nb_2O_5//activated carbon (□), Nb_2O_5//activated carbon (■), TiO_2(B)//activated carbon (●), $Li_4Ti_5O_{12}$/CNF//activated carbon (■) and hard carbon//activated carbon (▲). (d) relationship between capacitance retention and cycle number for T-Nb_2O_5//PANI-SWCNT supercapacitor device.

The galvanostatic charge-discharge tests of devices were performed from 0~3 V at various current densities. As shown

in Figure 5a and 5b, the charge-discharge curves of Ti doped T-Nb_2O_5//PANI-SWCNT and Ti doped T-Nb_2O_5//activated carbon devices both show well symmetric triangular shapes, which indicates well-defined capacitive energy storage behavior with balanced charge storage at both electrodes. The specific capcaitance of the supercapacitor device is calculated based on equation 4, where M is the total mass of positive and negative electrodes and ΔV is the device operation window. The specific capacitance of Ti doped T-Nb_2O_5//PANI-SWCNT device is calculated to be 88.27 F g^{-1} at 0.1 A g^{-1}, corresponding to the energy density of 110.3 Wh kg^{-1} at 150 W kg^{-1}. Meanwhile, the capacitance maintains 18.93 F g^{-1} at 2 A g^{-1}, which equals to 23.6 Wh kg^{-1} at 3 kW kg^{-1}. For Ti doped T-Nb_2O_5//activated carbon device, the specific capacitance is 43.33 F g^{-1} at 0.1 A g^{-1}. The energy density is only 52.9 Wh kg^{-1} at 150 W kg^{-1}. It is evident that the application of PANI-SWCNT is beneficial for enhancing the energy density of non-aqueous LIC.

To further illustrate the characteristics of the devices, the relationship between energy density and power density is plotted in the Ragone plot in Figure 5c. The energy density of this device is comparable with some lithium ion batteries. Meanwhile, the power density is greatly improved than batteries. Besides, the energy density of supercapacitor device is greatly enhanced by combining two high energy density materials at positive electrode and negative electrode. As a result, our device has much improved energy density comparing with some best organic electrolyte supercapacitor devices using activated carbon on one electrode, such as mesoporous Nb_2O_5//activated carbon (■, 48 Wh kg^{-1})[9], TiO_2(B)//activated carbon (●, 55 Wh kg^{-1}),[23] $Li_4Ti_5O_{12}$/CNF// activated carbon (■, 55 Wh kg^{-1})[4] and hard carbon//activated carbon (▲, 82 Wh kg^{-1}).[24]

The cycling stability is another important parameter for supercapacitors. As shown in Figure 5d, after 2000 cycles, the capacitance of device remains 71 %. This value is not yet satisfactory for practical application. The fast degradation of capacitance may partly come from the relative poor stability of PANI due to the shrinking and swelling during cycling,[25, 26] as shown in Figure S4. We believe the improvement in PANI's cycling stability will be beneficial for achieving better device cycling performance. Nevertheless, more future work in improving the cycling stability is highly desirable.

Conclusion

In conclusion, we developed a Ti doping strategy for T-Nb_2O_5 to preserve the high capacity with good long term stability. Meanwhile, the pseudocapacitive Li^+ ion storage behaviour is not affected by Ti doping. The origin of such improvement could come from the reduced charge transfer resistance and better electron conductivity during Li^+ insertion. Apart from Ti doped T-Nb_2O_5, PANI-SWNT is developed with high capacitance and good rate capability. As a result, Ti doped T-Nb_2O_5//PANI-SWCNT shows elevated energy density. The idea of replacing carbon material in LIC will be beneficial for developing future high energy density non-aqueous supercapacitors.

Acknowledgements

This work is supported by the National Research Foundation Competitive Research Programme, Award No. NRF-CRP-13-2014-02 and the Nanomaterials for Energy and Water Management Programme under the Campus for Research Excellence and Technological Enterprise (CREATE), that is supported by the National Research Foundation, Prime Minister's Office, Singapore.

Notes and references

‡ Footnotes relating to the main text should appear here. These might include comments relevant to but not central to the matter under discussion, limited experimental and spectral data, and crystallographic data.

1. P. Simon and Y. Gogotsi, *Nature materials*, 2008, **7**, 845-854.
2. K. Naoi, S. Ishimoto, J.-i. Miyamoto and W. Naoi, *Energy & Environmental Science*, 2012, **5**, 9363-9373.
3. Z. Chen, V. Augustyn, J. Wen, Y. Zhang, M. Shen, B. Dunn and Y. Lu, *Adv. Mater.*, 2011, **23**, 791-795.
4. K. Naoi, S. Ishimoto, Y. Isobe and S. Aoyagi, *Journal of Power Sources*, 2010, **195**, 6250-6254.
5. V. Aravindan, N. Shubha, W. C. Ling and S. Madhavi, *J. Mater. Chem. A*, 2013, **1**, 6145-6151.
6. V. Augustyn, J. Come, M. A. Lowe, J. W. Kim, P.-L. Taberna, S. H. Tolbert, H. D. Abruña, P. Simon and B. Dunn, *Nature materials*, 2013, **12**, 518-522.
7. J. W. Kim, V. Augustyn and B. Dunn, *Advanced EnergMaterials*, 2012, **2**, 141-148.
8. L. Kong, C. Zhang, S. Zhang, J. Wang, R. Cai, C. Lv, W. Qiao, L. Ling and D. Long, *Journal of Materials Chemistry A*, 2014, **2**, 17962-17970.
9. E. Lim, H. Kim, C. Jo, J. Chun, K. Ku, S. Kim, H. I. Lee, I.-S. Nam, S. Yoon, K. Kang and J. Lee, *ACS Nano*, 2014, **8**, 8968-8978.
10. L. L. Zhang and X. Zhao, *Chemical Society Reviews*, 2009, **38**, 2520-2531.
11. K. Zhang, L. L. Zhang, X. Zhao and J. Wu, *Chemistry of Materials*, 2010, **22**, 1392-1401.
12. Y. G. Wang, H. Q. Li and Y. Y. Xia, *Advanced Materials*, 2006, **18**, 2619-2623.
13. T. Ohzuku, K. Sawai and T. Hirai, *Journal of Power Sources*, 1987, **19**, 287-299.
14. X. Wu, J. Miao, W. Han, Y.-S. Hu, D. Chen, J.-S. Lee, J. Kim and L. Chen, *Electrochemistry Communications*, 2012, **25**, 39-42.
15. M. Sathiya, A. Prakash, K. Ramesha, J. M. Tarascon and A. Shukla, *Journal of the American Chemical Society*, 2011, **133**, 16291-16299.
16. X. Wang, G. Li, Z. Chen, V. Augustyn, X. Ma, G. Wang, B. Dunn and Y. Lu, *Advanced Energy Materials*, 2011, **1**, 1089-1093.
17. Z. Fan, J. Yan, T. Wei, L. Zhi, G. Ning, T. Li and F. Wei, *Advanced Functional Materials*, 2011, **21**, 2366-2375.

18. X. Lu, Z. Jian, Z. Fang, L. Gu, Y.-S. Hu, W. Chen, Z. Wang and L. Chen, *Energy & Environmental Science*, 2011, **4**, 2638-2644.
19. A. L. Viet, M. Reddy, R. Jose, B. Chowdari and S. Ramakrishna, *The Journal of Physical Chemistry C*, 2009, **114**, 664-671.
20. E. Song and J.-W. Choi, *Nanomaterials*, 2013, **3**, 498-523.
21. X. Wang, A. Sumboja, M. Lin, J. Yan and P. S. Lee, *Nanoscale*, 2012, **4**, 7266-7272.
22. X. Wang, W. S. Liu, X. Lu and P. S. Lee, *Journal of Materials Chemistry*, 2012, **22**, 23114-23119.
23. T. Brousse, R. Marchand, P.-L. Taberna and P. Simon, *Journal of Power Sources*, 2006, **158**, 571-577.
24. W. J. Cao and J. P. Zheng, *Journal of Power Sources*, 2012, **213**, 180-185.
25. G. A. Snook, P. Kao and A. S. Best, *Journal of Power Sources*, 2011, **196**, 1-12.
26. J. Yan, L. Yang, M. Cui, X. Wang, K. J. Chee, V. C. Nguyen, V. Kumar, A. Sumboja, M. Wang and P. S. Lee, *Advanced Energy Materials*, 2014, DOI: 10.1002/aenm.201400781, n/a-n/a.

TOC abstract

Developing high energy density supercapacitor is of great importance to the transportation, consumer electronics and micro-grid energy storage sectors. We introduce a new electrode combination with titanium-doped orthorhombic phase niobium oxide and polyaniline-single wall carbon nanotube. The organic electrolyte based supercapacitor achieves energy density over 110.3 Wh kg^{-1} at 150 W kg^{-1}.

ToC figure